International Journal of Hydrogen Energy 53 (2024) 200–207

Contents lists available at ScienceDirect

International Journal of Hydrogen Energy

journal homepage: www.elsevier.com/locate/he

CFD model of refuelling through the entire equipment of a hydrogen refuelling station

H. Ebne-Abbasi [*], D. Makarov, V. Molkov

Hydrogen Safety Engineering and Research Centre (HySAFER), Ulster University, Newtownabbey, BT37 0QB, Northern Ireland, UK

A R T I C L E I N F O

Handling Editor: D.-V. No. Vo

Keywords:
Hydrogen refuelling station (HRS)
Equipment of HRS
CFD model of refuelling
Model validation
Fuelling protocols
Hydrogen safety

A B S T R A C T

This paper aims at the development and validation of a computational fluid dynamic (CFD) model for simulations of the refuelling process through the entire equipment of the hydrogen refuelling station (HRS). The absence of such models hinders the design of inherently safer refuelling protocols for an arbitrary combination of HRS equipment, hydrogen storage parameters, and environmental conditions. The CFD model is validated against the complete process of refuelling lasting 195s in Test No.1 performed by the National Renewable Energy Laboratory (NREL). The test equipment includes high-pressure tanks of HRS, pressure control valve (PCV), valves, pipes, breakaway, hose, and nozzle all the way up to three onboard tanks. The model accurately reproduced hydrogen temperature and pressure through the entire line of HRS equipment. A standout feature of the CFD model, distinguishing it from simplified models, is the capability to predict temperature non-uniformity in onboard tanks, a crucial factor with significant safety implications.

1. Introduction

The European Union decided to ban the sale of new fossil-fuelled vehicles by 2035, while the UK is aiming to end the sale of new petrol and diesel cars and vans by 2030 [1]. Hydrogen is an emerging energy carrier for use in the transportation system which has demonstrated its efficacy as a promising substitute for fossil fuels. Hydrogen dispensing is an important and complex process that should consider the “customer acceptable experience” conditions to encourage the adaptation of the technology: acceptable refuelling time, a driving range of more than 500 km, technical and economical parity to fossil fuel technologies [2–4]. The US Department of Energy [5] and the European Clean Hydrogen Partnership [6] propose to target a 3-4-min duration for refuelling hydrogen-powered cars. To bear high working pressures, onboard tanks use carbon fibre-reinforced polymer (CFRP). These tanks feature a liner that limits permeation to a regulated level [7]. The integrity of onboard storage tanks is endangered during fuelling when they are exposed to high temperatures resulting from gas compression, e.g. from 2 MPa to 87.5 MPa, conversion of kinetic energy into internal energy [8], and lower thermal conductivity of the materials [9]. The fuelling protocols mentioned in SAE J2601 [10], SAE J2579 [11], ISO 15869 [12] and regulation GTR#13 [13], limit the allowable bulk hydrogen temperature in the tank between −40 °C and 85 °C, maximum fuelling pressure by 125 % of the nominal working pressure (NWP), and the state of charge (SoC) to 100 %. Exceeding these temperature thresholds may result in the degradation of the tank over time, and even sudden failure of the hydrogen tank, i.e. tank rupture or hydrogen leak [14,15]. A heat exchanger (HE) is used to pre-cool hydrogen and keep its temperature in the tank below the 85 °C threshold [16,17]. However, the pre-cooling complicates the fuelling station design, deteriorates its performance, worsens reliability and increases cost [18]. An ideal fuelling strategy should be able to direct the hydrogen fuelling process in a reasonable duration while keeping the temperature and pressure inside the tank within the limits and it should be able to reach an SoC of 90 %–100 % in different ambient conditions [19,20].

The SAE J2601 [10] fuelling protocol is limited to light-duty vehicles (LDV) that can store a maximum of 10 kg of hydrogen inventory. The SAE J2601-2 [21] offers only general safety guidelines for heavy-duty vehicles (HDV), not protocols. The same is valid for SAE J2601-3 [22] aimed to provide recommendations for fuelling hydrogen-powered industrial trucks like tractors, forklifts and pallet jacks, but, unfortunately, does not provide a technical specification of fuelling protocols. The development of a fuelling protocol is a rigorous and intricate process that demands the utilization of modelling tools and experimental validation [23].

Conducting numerous experiments to develop fuelling protocols for

* Corresponding author.
E-mail address: ebne_abbasi-h@ulster.ac.uk (H. Ebne-Abbasi).

https://doi.org/10.1016/j.ijhydene.2023.12.056
Received 12 May 2023; Received in revised form 4 September 2023; Accepted 7 December 2023
Available online 14 December 2023

arbitrary conditions is costly and impractical. So far, no conclusive and transparent fuelling protocol has been established for HDVs through experimental research. The use of thoroughly validated models of refuelling through the entire equipment of an HRS can greatly expedite the development of protocols and reduce associated costs by excluding numerous expensive and hazardous experiments [24]. To achieve this, contemporary models, i.e., CFD models, must be available. CFD is a contemporary research technique that allows one to gain an understanding of underlying physical phenomena. The advantages of CFD models compared to the reduced models include but are not limited to resolution of temperature non-uniformity in onboard storage versus average (bulk) temperature in the reduced integral models, simulation of equipment for which heat and mass transfer correlations are not yet available, etc. However, such CFD models are yet to be developed and thoroughly validated. One of the challenges for CFD models that is addressed in this work is simulation time [25]. There is no intention to incorporate CFD models into an automated fuelling system with a short response time, but the development with the use of validated CFD model protocols will close this issue.

So far, CFD models of hydrogen refuelling are focused only on the thermal behaviour of a hydrogen tank system. In many cases, due to the high computational cost of CFD simulations, reduced models are developed and used. The most of reduced models are focused on the thermodynamical state of onboard tanks only [18,23,24,26–30]. In 2014 Schneider et al. developed the software H2-Fill [31] which calculates pressure and temperature in the onboard tank only while assuming uniform temperature distribution in the tank [32]. In 2015 Air Liquide's team published model SOFIL [18,25] that assumes homogeneous gas temperature inside the onboard tank and solves mass and energy conservation equations for the piping only from the dispenser to the onboard tank. The Engie Lab CRIGEN developed the modelling tool Hyfill to simulate the fast filling and emptying of hydrogen tanks and predict the final hydrogen bulk temperature in a tank [23]. Engie's Hyfill is based on the MATLAB/Simulink software and, being a pseudo-1D model, it assumes uniform hydrogen temperature distribution in onboard tanks [23]. It is limited to modelling the gas dynamics from the dispenser to the onboard tanks and 1D heat transfer between the gas and the outside [23]. It is worth noting that these models are industrial models and are not publicly available. There is only one model to the best knowledge of authors that is publicly available and does include the entire equipment of an HRS: the reduced model H2FillS developed in 2021 by Kuroki et al. [33]. This reduced model is based on the Hydrogen Refuelling Station Dynamic Simulation (HRSDS) software of Kyushu University. It can estimate thermodynamic parameters at different HRS locations. However, as an integral model, it still has limitations which cannot be overcome without contemporary CFD models. These include the inability to model HRS's high pressure (HP) tanks thermal behaviour during fuelling, to assess the non-uniformity of hydrogen temperature in onboard storage tanks and difference in temperature in materials of the onboard tank, etc.

CFD models can surpass these limitations, provide deeper insight into underlying physical phenomena, and simulate the combined impact of diverse equipment of HRS on heat and mass transfer during fuelling to develop efficient refuelling protocols, including those without precooling. CFD models are usually associated with high 1computational costs. As a result, all CFD studies of hydrogen fuelling, to mention a few [8,16–18,32,34–38], were focused on the thermal behaviour of onboard tanks only and did not account for processes of heat and mass transfer in the entire refuelling line equipment at HRS [39]. In 2018 Bourgeois et al. [39] stressed the importance of considering the entire fuelling line when studying the fuelling procedure. To develop effective and safe refuelling protocols, it is crucial to include all components of HRS involved in the process into consideration.

The current study is the follow-up of the author's previous work in which a CFD model has been validated for the startup phase of the fuelling process [40]. It aims to validate the CFD model against the whole duration of the fuelling process of 195 s in Test No.1 performed in 2021 in NREL by Kuroki et al. [33].

2. Validation experiment: NREL Test No.1

The experiment used in this study for the CFD model validation was performed at the Hydrogen Infrastructure Research Facility of NREL by Kuroki et al. [33]. Fig. 1 presents the piping and instrumentation diagram (PID) of the fuelling line components. The temperature was measured in several locations: in each of two HP tanks (TE1) that were changed once during fuelling, before and after the PCV (TE2 and TE3), after the HE (TE4), and in the centre of two of the onboard tanks (TE5 and TE6) with an accuracy of ± 1.5 K. The pressure was also measured at the exit of the HP tanks (PT1), before valve 4 (PT2) and at one of the onboard tanks with an accuracy of ± 1.0 MPa [33]. The hydrogen flows from one of two 300-L HP tanks, through almost 62 m of pipe with 24 bends (90-degree), PCV, mass flow rate meter (MFM), HE, breakaway, hose, nozzle and 5 other valves to the three 36-L onboard storage tanks. The length-to-diameter (L/D) ratio of the onboard tanks is reported as 3.4 and is unknown for HP tanks. The dimensions, materials and thermal properties for each piping section are available in the appendix section of the experimental paper [33].

Two tests were carried out by the experimentalists [33]. Test. No.1 was performed without any leak checks. Test No.2 was done along with a leak check at the start-up phase and two leak checks during the main fuelling phase. The simulation of the start-up phase during the Test. No.2 is reported in our previous study [40]. Test No.1 was selected in this study to validate the main fuelling process simulations. The initial temperature, pressure, and average pressure ramp rate (APRR) for Test No.1 are shown in Table 1.

3. CFD model

3.1. Calculation domain and parameters of HRS components

Fig. 2 presents the calculation domain geometry that exactly follows the experimental PID shown in Fig. 1. The only reported parameter for the HP tanks is a volume of 300 L each [33]. The HP tanks are assumed to be cylinders. The HP tank L/D ratio was assumed to be 3 and its total wall thickness was estimated as 33 mm combined of linear and CFRP. The pipe's dimensions, i.e., length, internal and external diameter, and thermal properties, i.e., density, thermal conductivity, and specific heat, are the ones that were provided by the experimentalists. The total length of piping is 62 m which includes 24 bends of 90° exaclty the same as the experiment (see Fig. 2). Static valves are fully open during refuelling. Due to the inherently complex geometry of PCV, MFM and valves, they are modelled as pipes of 10 cm lengths with the equivalent internal diameters (ID) calculated using the flow coefficient reported in Ref. [33] following the procedure described in Ref. [40].

Table 2 shows the IDs of the HRS components.

The thermal mass of the valves, PCV and MFM was not reported in Ref. [33]. Thus, the external diameter of the "numerical valves" is assumed to be equal to their upstream pipes. It is worth noting that the thermal conductivity of the breakaway and the nozzle were not

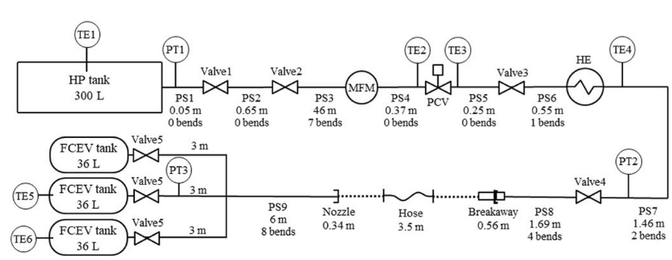

Fig. 1. PID of the NREL experimental facility.

Table 1
Experimental conditions of Test No.1 [33].

$T_{initial}$ (ambient)	$T_{initial}$ (HP tank)	$P_{initial}$ (upstream of PCV)	$P_{initial}$ (downstream of PCV)	APRR
23.0 °C	17.5 °C	88.0 MPa	6 MPa	19.8 MPa/min

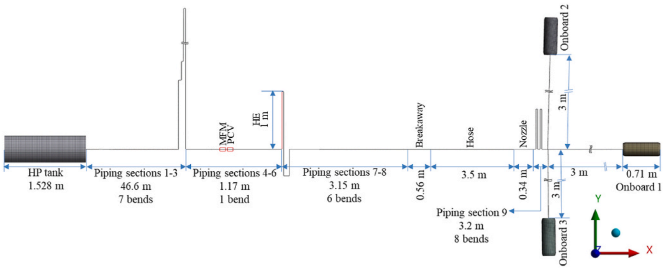

Fig. 2. The calculation domain (top view).

elucidated experimentally and analytically, but were estimated by the experimentalists based on the temperature rise of hydrogen flowing from the breakaway inlet to the nozzle exit [33]. The length and internal diameter of the breakaway, hose and nozzle are the same as those of the experiment, but their external diameter is adjusted and reported by the experimentalists to match the real weight of each component [33]. The specification of the piping section from the manifold to the onboard tanks is not reported in Ref. [33] but it is assumed to be the same as in the H2Fills software demonstration example which is replicating the NREL refuelling station [33].

The geometry of the manifold was not reported by the experimentalists. In the simulations, a manifold was designed to split the flow from the 5.1 mm upstream pipe into three similarly sized 5.1 mm pipes leading to three onboard tanks. The dimensions and the isometric view of the designed manifold for simulations are given in Fig. 3. In the lack of information for the manifold, its wall thickness and its material are assumed to be the same as its upstream pipes (2.2 mm), and its total length is considered to be 100 mm.

The computational grid is composed of 207,252 hexahedral control volumes (CV). The minimum orthogonal quality of the mesh is 0.7 with an average quality of 0.97. The sensitivity analysis for mesh is presented in the next section.

3.2. Governing equations and numerical details

The governing equations that are used in the CFD model are the unsteady three-dimensional Favre-averaged mass, momentum and energy conservation equations [41] respectively as follows:

$$\frac{\partial \overline{\rho}}{\partial t}+\frac{\partial}{\partial x_j}\left(\overline{\rho}\widetilde{u}_j\right)=0, \tag{1}$$

$$\frac{\partial}{\partial t}\left(\overline{\rho}\widetilde{u}_i\right)+\frac{\partial}{\partial x_j}\left(\overline{\rho}\widetilde{u}_j\widetilde{u}_i\right)=-\frac{\partial \overline{p}}{\partial x_i}+\frac{\partial}{\partial x_j}\left(\mu+\mu_t\right)\left(\frac{\partial \widetilde{u}_i}{\partial x_j}+\frac{\partial \widetilde{u}_j}{\partial x_i}-\frac{2}{3}\frac{\partial \widetilde{u}_k}{\partial x_k}\delta_{ij}\right)+\overline{\rho}g_i, \tag{2}$$

$$\frac{\partial}{\partial t}\left(\overline{\rho}\widetilde{E}\right)+\frac{\partial}{\partial x_j}\left(\widetilde{u}_j\left(\overline{\rho}\widetilde{E}+\overline{p}\right)\right)=\frac{\partial}{\partial x_j}\left(\left(\lambda+\frac{\mu_t c_p}{Pr_t}\right)\frac{\partial \widetilde{T}}{\partial x_j}\right). \tag{3}$$

where x_i,x_j,x_k are the Cartesian coordinates, u_i, u_j, u_k are the velocity components, t is the time, p is the pressure, ρ is the density, g_i is the gravity acceleration in i-axis direction, μ and μ_t are the molecular and turbulent dynamic viscosity respectively, δ_{ij} is the Kronecker symbol, E is the total energy, T is the temperature, c_p is the specific heat at constant pressure, λ is the thermal conductivity, Pr_t is the turbulent Prandtl number. The symbol "overbar" stands for Reynolds averaged parameters and "tilde" for Favre averaged parameters.

Flow turbulence was modelled using the standard k-ε turbulence model [42]:

$$\frac{\partial(\overline{\rho}\overline{k})}{\partial t}+\frac{\partial}{\partial x_j}\left(\overline{\rho}\widetilde{u}_j\overline{k}\right)=\frac{\partial}{\partial x_j}\left(\left(\mu+\frac{\mu_t}{\sigma_k}\right)\frac{\partial \overline{k}}{\partial x_j}\right)+G_k+G_b-\overline{\rho\varepsilon}, \tag{4}$$

$$\frac{\partial(\overline{\rho\varepsilon})}{\partial t}+\frac{\partial}{\partial x_j}\left(\overline{\rho}\widetilde{u}_j\overline{\varepsilon}\right)=\frac{\partial}{\partial x_j}\left(\left(\mu+\frac{\mu_t}{\sigma_\varepsilon}\right)\frac{\partial \overline{\varepsilon}}{\partial x_j}\right)+C_{1\varepsilon}\frac{\overline{\varepsilon}}{k}\left(G_k+C_{3\varepsilon}G_b\right)-C_{2\varepsilon}\overline{\rho}\frac{\overline{\varepsilon}^2}{k}, \tag{5}$$

where k is the turbulent kinetic energy, ε is the dissipation rate of turbulent kinetic energy, $\mu_t = \overline{\rho}c_\mu\overline{k}^2/\overline{\varepsilon}$, $G_K = \mu_t S^2$, $G_b = -g_i(\mu_t/\overline{\rho}Pr_t)(\partial\overline{p}/\partial x_i)$, $c_m = 0.09$, $\sigma_k = 1.0$, $\sigma_e = 1.3$, $C_{1\varepsilon} = 1.44$, $C_{2\varepsilon} = 1.92$, $C_{3\varepsilon} = tanh\left|\widetilde{u}_y/\left(\widetilde{u}_x^2+\widetilde{u}_z^2\right)^{0.5}\right|$, $S=\sqrt{2\overline{S}_{ij}\overline{S}_{ij}}$ is the mean rate of strain, $\overline{S}_{ij} = \frac{1}{2}\left(\frac{\partial \overline{u}_i}{\partial x_j}+\frac{\partial \overline{u}_j}{\partial x_i}\right)$.

Standard wall functions [42] have been employed for velocity (no-slip condition), temperature, turbulent kinetic energy and dissipation rate on solid surfaces. Buoyancy effects were also considered in the model by applying the gravitational acceleration normal to the ground surface. As the ideal gas model cannot accurately predict pressure

Table 2
Calculated equivalent internal diameter of valves, PCV, HE, and MFM using C_v from Ref. [33].

PID component	Valve1	Valve2	MFM	PCV	Valve3	HE	Valve4	Valve5
Flow coefficient, C_v [33]	1.3	0.75	1.0	1.0	0.75	1.0	0.75	1.0
Calculated equivalent ID [mm]	6.5	4.99	5.76	5.76	4.99	5.76	4.99	5.76

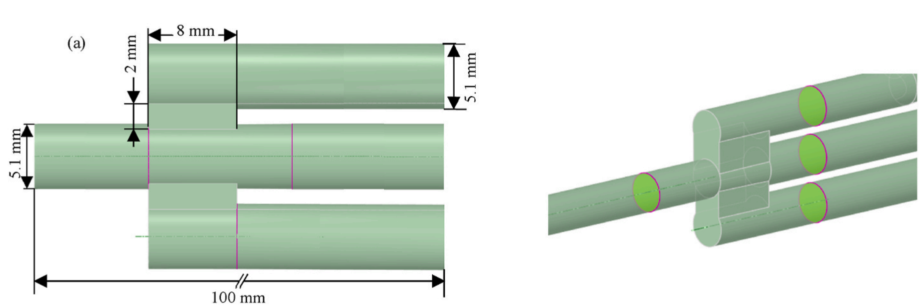

Fig. 3. Manifold model: plane view (left) and isometric view (right).

behaviours at high pressures, the National Institute of Standards and Technology (NIST) real gas model was applied. This model uses the NIST Thermodynamic and Transport Properties of Refrigerants and Refrigerant Mixtures Database Version 7.0 (REFPROP v7.0) [43] to evaluate the transport and thermodynamic properties of fluids. An implicit, pressure-based solver was used in the simulations, the SIMPLE algorithm was applied for pressure-velocity coupling with the first-order accurate time stepping. Convective terms were discretised using the first-order upwind numerical scheme, and diffusion terms – using the central-difference scheme. Convergence was controlled in each time step using the root mean square (RMS) residual for mass and momentum conservation equations, which were set to 10^{-6}.

Timestep and mesh sensitivity analysis were done in line with the CFD model evaluation protocol [44]. Timestep equal to TS = 10^{-3} s was applied at the initial stages of the simulation (up to 1 s) and then it was increased with the simulation advancement to see how it affects the results. The temperature in onboard tank 1 is measured. The temperature starts to deviate at timestep sizes larger than 0.05 s (Fig. 4-Left). Fig. 4 (right) shows the sensitivity analysis for the mesh. Three different meshes were created: one coarse mesh with 104,375 CVs, one with 207, 252, and a fine one with 540,849 CVs. The temperature in the onboard tank 1 is compared for these cases. The result for coarse mesh deviates from the results of the experiment and the rest of the simulations. For saving computational resources, the case with 207K CVs is selected for this study.

The heat conduction through the walls is modelled using the "shell conduction" capability of ANSYS Fluent. This tool calculates conjugate heat transfer through the walls in both parallel and normal directions to the walls [45]. The model accounts for the thermal properties, thickness, and external convective heat transfer. The external convective heat transfer coefficient value of 7 W/m^2/K is used in line with the study [9].

All walls are modelled as impermeable and non-slip boundaries. The initial conditions are those in the experiment (see Table 1): the pressure is 88 MPa in the HP tanks and down to the PCV, 6 MPa from the PCV and down to the onboard tanks, initial temperature is 17.5 °C in the HP tank and its walls and 23 °C for the rest of the domain.

The experimental procedure of switching HP tanks in the simulations was emulated by stopping the simulation at the specified pressure of 63.5 MPa (achieved at time 121.5 s) and re-initialising ("patching") the temperature and pressure inside the HP tank and the temperature for the HP tank walls to the initial values.

The simulations were performed using ANSYS Fluent 2020R2 as a CFD engine [45]. The CFD simulations of 195 s of the main fuelling phase take about 2 days on a 32-core AMD Opteron CPU running at 2.3 GHz.

3.3. Modelling PCV and HE

Experimentally measured pressure downstream of PCV (PT2, located after HE) and temperature immediately after HE (TE4) were simulated by special means described in this section. They were used as CFD model input parameters driving the solution of momentum and energy equations to avoid computationally expensive resolution of flow through PCV and HE. It must be mentioned that the PT2 sensor is located downstream of PCV, after 2.25 m of pipes and HE, in which the experimental length of HE is unknown and simulated HE is assumed to be 1 m.

In the described CFD model a strategy was implemented to control the pressure in the PCV valve via assigning velocity magnitude in the PCV control volumes (the momentum conservation equations were not solved in those control volumes). An in-house code was developed to control pressure downstream of PCV (at PT2 location) by changing velocity at PCV at each time step (implemented as a user-defined function capability of ANSYS Fluent). The procedure is presented in Fig. 5 and works as follows:

1. Simulated pressure p_{sim} downstream of PCV (at PT2) is acquired from Fluent,
2. Pressure p_{sim} is compared with the experimental pressure p_{exp} downstream of PCV (PT2),
3. Dimensionless parameter dp_{norm} is calculated by Eq. (6), and
4. PCV velocity at the previous time step V_{i-1} is multiplied by dp_{norm}, after which
5. The current time PCV velocity value is assigned ($V_{i-1} = V_i$),

and the whole process is called again at the next time step. The dimensionless parameter dp_{norm} is the departure of simulated pressure (p_{sim}) from the experimental one (p_{exp}) introduced as follows:

$$dp_{norm} = 1 - \frac{p_{sim} - p_{exp}}{p_{exp}}. \tag{6}$$

Details of the cooling system (HE) are not available in the experimental paper [33]. For the modelling purpose, the HE was represented as a 1.0 m long pipe section with an equivalent internal diameter calculated based on the available HE flow coefficient. A similar to the above strategy was implemented here for temperature: temperature in control volumes representing HE was assigned to the temperature measured in the experiment. Fig. 6 illustrates how the pressure and temperature control strategies were successful in the reproduction of the experimental data as input for CFD simulations. Fig. 6 (left) compares the dynamics of the experimental pressure downstream of PCV (measured in PT2 in PID, Fig. 1) with the simulated pressure at the same spot location. Fig. 4 (right) compares the experimental temperature after the pre-cooler (measurement location TE4 in PID, Fig. 1) with the simulated temperature at the same spot. As expected, the simulated parameters practically coincide with the experimental ones. It should be noted that the pressure regulation technique described in Fig. 4 controls pressure with an accuracy of ±1 % and any visible deviations are due to the numerical errors in digitising the experimental data and adding a trendline for the digitized data.

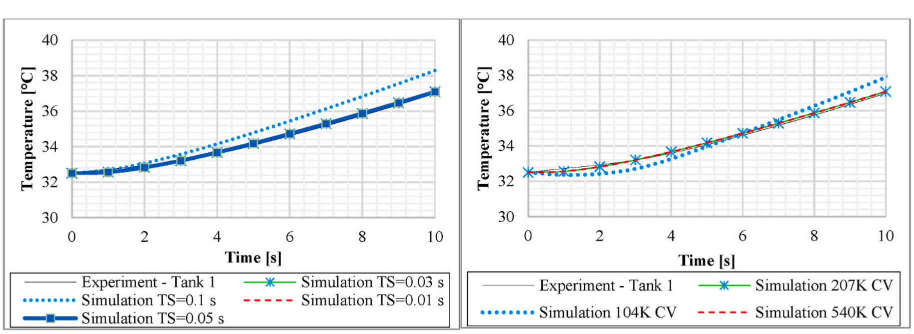

Fig. 4. Results for timestep (TS) independency analysis: (Left) pressure in the onboard tank 1 and (Right) temperature in onboard tank 1.

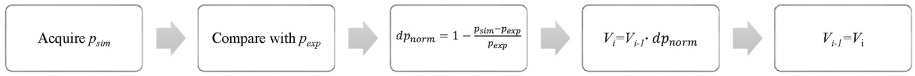

Fig. 5. Procedure to control pressure downstream of PCV by prescribing flow velocity in “numerical PCV”.

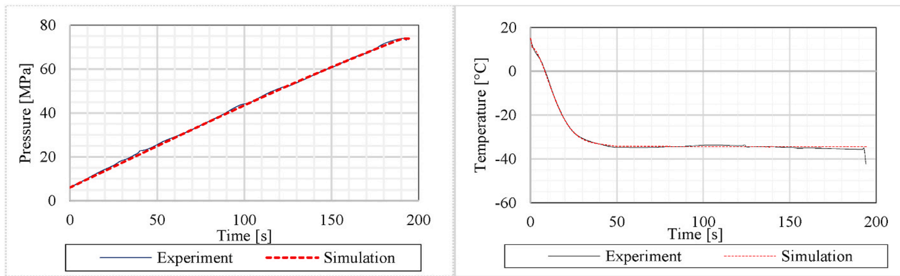

Fig. 6. Experimental and simulated pressure at PT2 (left); experimental and simulated temperature after HE at TE4 (right).

4. Simulation results and discussion

The experimental data of Test No.1 were digitized from the graphs in the paper [33] to enable comparison with simulation results. Fig. 7 (left) shows the dynamics of experimental and simulated pressure in onboard tanks 1 and 2. The experimental pressure is measured at the tank inlet, and it is assumed with good confidence that the pressure in the tank is equal to the pressure in the inlet. In the simulations, the pressure was measured in the same location. The simulated pressure inside the tank was indeed the same as the pressure in the inlet. The simulated pressure reproduces the experimental one with a difference of less than ±1 % across the whole fuelling duration which is well within the pressure transducer accuracy of ±1 MPa. The difference in simulated pressure in Tank 1 and Tank 2 is less than 1 % and is, most likely, due to the difference in pressure losses in manifolds of different geometry.

The location of thermocouples in the experiment (TE5 and TE6) is referred to as tanks centre positions [33]. In the simulations, the temperature was measured on the tank’s axes and is located in the centre of each tank as is depicted in Fig. 8.

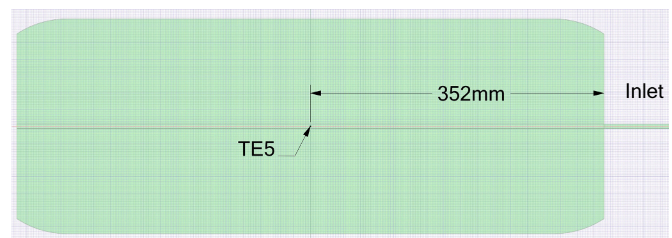

Fig. 8. Location of temperature sensor (TE5) in onboard tank 1.

Fig. 7 (right) compares experimental and simulated temperatures in Tank 1 and Tank 2. The simulated temperatures are in good agreement with experimental measurements for both tanks (thermocouples TE5 and TE6) for the whole duration of the fuelling process with a deviation of less than 5 °C. The small error in the prediction of temperature in the onboard tanks might be due to simplifications in modelling valves, PCV and MFM, as their thermal masses are not taken into account [33] due to lack of available experimental data. So, these components do not absorb enough heat during fuelling. Besides, the experimentalists estimated the thermal conductivity of materials based on the thermal rise of hydrogen while passing through the components. This method may not yield highly accurate results as there might be some uncertainty during measurements. The uncertainty includes: the turbulence within the hydrogen flow can complicate the heat transfer process to the sensors and introduce some more complexities that could affect the accuracy of the methodology, at some component interfaces and near walls, the behaviour of flow can significantly differ from bulk conditions, which contributes to uncertainties in thermal rise measurements, and the experiment might not fully take account for heat losses to the environment, potentially resulting in an underestimation of the true thermal conductivity values. Overall, these results validate the CFD model’s capability to accurately predict hydrogen temperature in the tank during the fuelling. As the initial and boundary conditions for both tanks are the same, the difference between the measured temperature in the two tanks is assumed to be the difference in pressure losses in manifolds of different geometry, as mentioned in the previous section.

Fig. 9 (left) shows pressure and temperature dynamics in the HP tanks of HRS. The simulation results for HP tank pressure and temperature follow closely the experimental results with a maximum deviation of less than 1 %. The maximum temperature deviation is right before the change of tanks and is −3 °C. The results could have been improved if the real geometry of the HP tank, its L/D, and the wall thicknesses were known. Besides, the thermal properties of liner and CFRP for the HP tanks are assumed to be similar to the ones used in the onboard tanks, which in real might be different. Fig. 9 (right) shows experimental and

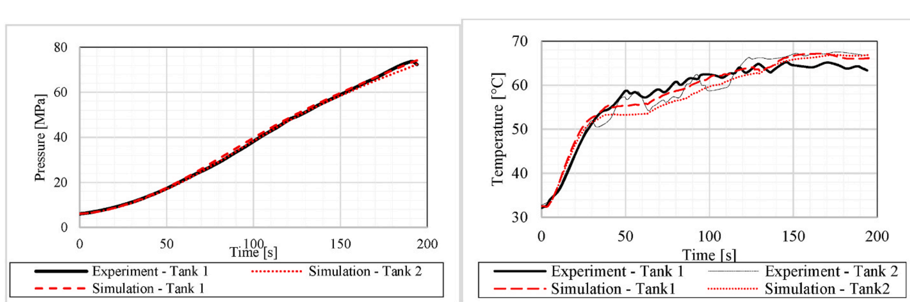

Fig. 7. Experimental and simulated pressures in onboard tanks (left). Experimental (TE5 and TE6) and simulated temperatures in the onboard tanks (right).

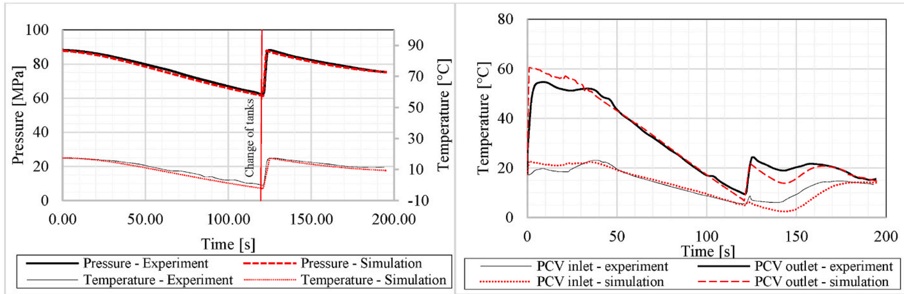

Fig. 9. Experimental and simulated pressure and temperature in the HP tanks (left). Experimental and simulated temperature upstream (TE2) and downstream (TE3) of the PCV (right).

simulated hydrogen temperatures before and after the PCV. The temperature increase after passing the PCV is due to the Joule-Thomson effect: at the pressure and temperature of filling, hydrogen has a negative Joule-Thomson coefficient causing the temperature increase (TE2 and TE3) while its pressure decreases in the PCV [33]. Because the exact locations of thermocouples TE2 and TE3 in the experiment were not reported, the difference in temperature at various locations from PCV was estimated from the simulations. It was found that the hydrogen temperature difference at distances from 5 cm to 20 cm from PCV is within negligible 0.1°. This is in line with the comment of experimentalists that temperature difference along the pipe length for less than 10 cm is negligible [46]. The CFD model reproduces the experimental temperature rise as hydrogen passes the PCV well with a maximum deviation within ±5 °C. The maximum deviation of the temperature happens after the tank change. The reason for that is probably due to the lower simulated temperature at the HP tank, which cooled down the fuelling line more (compared to the experiment) and lowered the inlet temperature which ended in a lower outlet temperature in the PCV. Plus, as mentioned before, the thermal mass of valves, PCV and MFM is not taken account, which can adversely affect the results. It is likely that if the HP tanks were modelled using their actual dimensions and materials, the results in the PCV could have been improved further. Yet, the simulations results for these parameters are well within the acceptable engineering accuracy for such a complicated process of heat and mass transfer.

The CFD model enables us to plot and analyse the pressure distribution along the centreline of the pipes. Fig. 10 depicts the distribution of pressure along the centreline of the pipes starting from the HP tank, across the system pipes and components, and up to the onboard tank 1 at different times - at the start of fuelling ($t = 0$ s), before changing the HP tank ($t = 124$ s) and at the end of fuelling ($t = 195$s). As can be seen, the main pressure drop happens in PCV in which the pressure is controlled in the fuelling line. Also, the pressure drop in the fuelling line is highest in the middle of the fuelling process (see pressure distribution at $t = 124$s) when the mass flow rate in the pipeline is large too.

Fig. 11 compares experimental and simulated mass flow rates across the PCV. The difference, i.e., oscillations, between measured and simulated mass flow rates can be attributed to the fact that the experimental mass flow rate was obtained from the measurements of the HP tank mass. In simulations, the mass flow rate is calculated in the MFM location, although measuring it in the PCV or other locations showed no difference. The simulated mass flow rate closely follows the experimental data trend.

As mentioned before, the developed CFD modelling approach is capable of simulating the effect of hydrogen inflow jet on temperature distribution and non-uniformity in the tank. This is especially important for hydrogen storage tanks with large L/D ratios [38,47]. In this study, the temperature non-uniformity was measured. The difference between the maximum spatial temperature and measured temperature in the temperature sensor location in tank 1 is shown in Fig. 12 (left). As is shown in Fig. 12 (left), the temperature non-uniformity in this tank can reach up to 7 °C. The situation will drastically change for larger L/D tanks, where non-uniformity can increase to unacceptable from the safety point of view 25–30° [47]. This is a serious issue for emerging conformable tanks for onboard storage.

5. Conclusions

The *originality* of this work is in the development and validation of the first of its kind CFD model which could simulate the entire HRS process with all its components. The model includes HP tanks, all the pipes and bends, MFM, PCV, HE, breakaway, hose and nozzle up to three separate onboard tanks. The simulations were performed using ANSYS Fluent as a computational engine and the in-house developed code to control flow through the PCV and temperature after the HE. The model

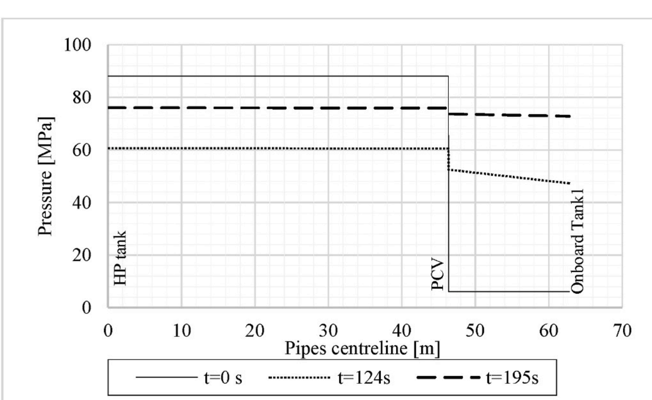

Fig. 10. Distribution of pressure across the centreline of the pipes at different times: (1) At the start of fuelling (t = 0s), (2) Before changing the HP tank, and (3) At the end of fuelling (t = 195s).

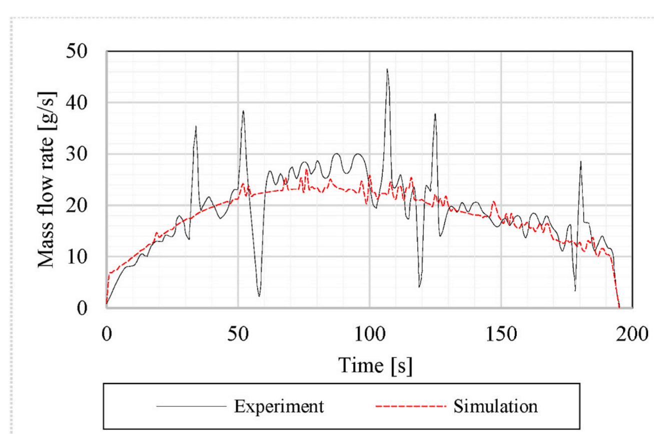

Fig. 11. Comparison of experimentally measured and simulated mass flow rate.

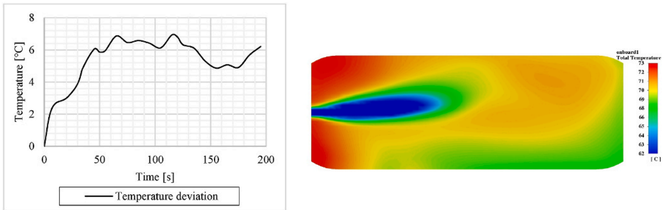

Fig. 12. (Left) The difference between maximum spatial temperature and measured temperature in the temperature sensor location in tank1 and (Right) temperature distribution in the onboard tank1 at the end of refuelling (t = 195s).

is highly flexible so that every component of the system can be modified and/or changed to perform parametric studies to get insights into underlying physical phenomena of heat and mass transfer. The benefit of the CFD model compared to reduced models is the capability to assess temperature non-uniformity inside onboard storage tanks to prevent their failure during refuelling.

The *significance* of this study is in the affordable time of simulations that can be used to develop fuelling protocols for arbitrary parameters of HRS equipment, onboard tanks and atmospheric conditions. This CFD model simulates 3 min fuelling process in only 2 days on a 32-cores CPU. The model can be used for designing fuelling protocols for the whole range of hydrogen-powered vehicles for road, rail, marine and aeronautical applications.

The *rigour* of this work is in the validation of the CFD model simulations against the unique refuelling experiment of NREL (Test No.1) through the entire equipment of HRS. The model can help to improve the accuracy and efficiency of refuelling simulations, leading to safer and more cost-effective hydrogen fuelling protocols.

The model will be validated against new experiments of fuelling as soon as they are made available and used as a contemporary tool for fuelling protocol development. The knowledge acquired during this study will be applied to LH2 fuelling/bunkering.

Disclaimer

Co-funded by the European Union. Views and opinions expressed are however those of the author(s) only and do not necessarily reflect those of the European Union or the Clean Hydrogen Partnership. Neither the European Union nor the Clean Hydrogen Partnership can be held responsible for them.

Declaration of competing interest

The authors declare that they have no known competing financial interests or personal relationships that could have appeared to influence the work reported in this paper.

Acknowledgements

This research has received funding from the Engineering and Physical Sciences Research Council (EPSRC) of the UK for funding through the EPSRC Centre for Doctoral Training in Sustainable Hydrogen "SusHy" (Grant EP/S023909/1), UK National Clean Maritime Research Hub funded by EPSRC grant EP/Y024605/1, and the Fuel Cells and Hydrogen 2 Joint Undertaking (now Clean Hydrogen Partnership) under the European Union's Horizon 2020 research and innovation programme through the SH2APED project under grant agreement No.101007182. Simulations were performed using the Tier 2 High-Performance Computing resources provided by the Northern Ireland High-Performance Computing (NI-HPC) facility, funded by the EPSRC (grant EP/T022175/1, https://www.ni-hpc.ac.uk/Kelvin2/(accessed on 1st Aug 2023)).

References

[1] UK HM Government. The ten point plan for a green industrial revolution. UK dep business. Energy Ind Strateg 2020:1–32.
[2] Genovese M, Cigolotti V, Jannelli E, Fragiacomo P. Hydrogen refueling process: theory, modeling, and in-force applications. Energies 2023;16:2890. https://doi.org/10.3390/en16062890.
[3] Muratori M, Bush B, Hunter C, Melaina M. Modeling hydrogen refueling infrastructure to support passenger vehicles. Energies 2018;11:1171. https://doi.org/10.3390/en11051171.
[4] Kang JE, Brown T, Recker WW, Samuelsen GS. Refueling hydrogen fuel cell vehicles with 68 proposed refueling stations in California: measuring deviations from daily travel patterns. Int J Hydrogen Energy 2014;39:3444–9. https://doi.org/10.1016/j.ijhydene.2013.10.167.
[5] Us DOE. Target explanation document: onboard hydrogen storage for light-duty fuel cell vehicles. US Drive 2017;1–29.
[6] Fuel Cells and hydrogen Joint undertaking (FCH JU). Multi-Annual Work Plan 2014-2020; 2014.
[7] Dadashzadeh M, Kashkarov S, Makarov D, Molkov V. Risk assessment methodology for onboard hydrogen storage. Int J Hydrogen Energy 2018;43:6462–75. https://doi.org/10.1016/j.ijhydene.2018.01.195.
[8] De Miguel N, Acosta B, Baraldi D, Melideo R, Ortiz Cebolla R, Moretto P. The role of initial tank temperature on refuelling of on-board hydrogen tanks. Int J Hydrogen Energy 2016;41:8606–15. https://doi.org/10.1016/j.ijhydene.2016.03.158.
[9] Simonovski I, Baraldi D, Melideo D, Acosta-Iborra B. Thermal simulations of a hydrogen storage tank during fast filling. Int J Hydrogen Energy 2015;40:12560–71. https://doi.org/10.1016/j.ijhydene.2015.06.114.
[10] Fuel Cell Standards Committee. J2601_202005, fueling protocols for light duty gaseous hydrogen surface vehicles. Rev 2020. SAE Int 2020:1–2. https://doi.org/10.4271/J2601_202005.
[11] Fuel Cell Standards Committee. J2579_201806 standard for fuel systems in fuel cell and other hydrogen vehicles. SAE International Technical Paper; 2018. https://doi.org/10.4271/J2579_201806.
[12] ISO/TS 15869 Gaseous hydrogen and hydrogen blends — land vehicle fuel tanks. https://www.iso.org/standard/52871.html. [Accessed 2 April 2023].
[13] United Nations Economic Commission for Europe. Global registry Geneva Switzerland ., 13. A 13: GTRN. Global technical regulation on hydrogen and fuel cell vehicles. 2013.
[14] Sun K, Li Z. Development of emergency response strategies for typical accidents of hydrogen fuel cell electric vehicles. Int J Hydrogen Energy 2021;46:37679–96. https://doi.org/10.1016/j.ijhydene.2021.02.130.
[15] Lazarenko O, Parkhomenko V-P, Sukach R, Bilonozhko B, Kuskovets A. Design features and hazards of hydrogen fuel cell cars. Fire Saf 2021;37:52–7. https://doi.org/10.32447/20786662.37.2020.08.
[16] Zheng J, Guo J, Yang J, Zhao Y, Zhao L, Pan X, Ma J, Zhang L. Experimental and numerical study on temperature rise within a 70 MPa type III cylinder during fast refueling. Int J Hydrogen Energy 2013;38:10956–62. https://doi.org/10.1016/j.ijhydene.2013.02.053.
[17] Melideo D, Baraldi D, Galassi MC, Ortiz Cebolla R, Acosta Iborra B, Moretto P. CFD model performance benchmark of fast filling simulations of hydrogen tanks with pre-cooling. Int J Hydrogen Energy 2014;39:4389–95. https://doi.org/10.1016/j.ijhydene.2013.12.196.
[18] Bourgeois T, Brachmann T, Barth F, Ammouri F, Baraldi D, Melideo D, Acosta-Iborra B, Zaepffel D, Saury D, Lemonnier D. Optimization of hydrogen vehicle refuelling requirements. Int J Hydrogen Energy 2017;42:13789–809. https://doi.org/10.1016/j.ijhydene.2017.01.165.
[19] Reddi K, Elgowainy A, Rustagi N, Gupta E. Impact of hydrogen refueling configurations and market parameters on the refueling cost of hydrogen. Int J Hydrogen Energy 2017;42:21855–65. https://doi.org/10.1016/j.ijhydene.2017.05.122.
[20] Reddi K, Elgowainy A, Rustagi N, Gupta E. Impact of hydrogen SAE J2601 fueling methods on fueling time of light-duty fuel cell electric vehicles. Int J Hydrogen Energy 2017;42:16675–85. https://doi.org/10.1016/j.ijhydene.2017.04.233.
[21] SAE International. SAE J2601-2 - fueling protocol for gaseous hydrogen powered heavy duty vehicles. SAE Int 2014. https://doi.org/10.4271/J2601/2_201409.
[22] SAE International. SAE J2601-3 - Fueling protocol for gaseous hydrogen powered industrial trucks. SAE International Technical Paper; 2022. https://doi.org/10.4271/J2601/3_201306.
[23] Charolais A, Ammouri F, Vyazmina E, Nouvelot Q, Guewouo T, Greisel M, Gebhard M, Kuroki T, Mathison S. Protocol for heavy duty hydrogen refueling: a modeling benchmark. Int Conf Hydrog Saf 2021:1150–60.
[24] Molkov V, Dadashzadeh M, Makarov D. Physical model of onboard hydrogen storage tank thermal behaviour during fuelling. Int J Hydrogen Energy 2019;44:4374–84. https://doi.org/10.1016/j.ijhydene.2018.12.115.
[25] Bourgeois T, Ammouri F, Weber M, Knapik C. Evaluating the temperature inside a tank during a filling with highly-pressurized gas. Int J Hydrogen Energy 2015;40:11748–55. https://doi.org/10.1016/j.ijhydene.2015.01.096.
[26] Hosseini M, Dincer I, Naterer GF, Rosen MA. Thermodynamic analysis of filling compressed gaseous hydrogen storage tanks. Int J Hydrogen Energy 2012;37:5063–71. https://doi.org/10.1016/j.ijhydene.2011.12.047.
[27] Bai Y, Zhang C, Duan H, Jiang S, Zhou Z, Grouset D, Zhang M, Ye X. Modeling and optimal control of fast filling process of hydrogen to fuel cell vehicle. J Energy Storage 2021;35:102306. https://doi.org/10.1016/j.est.2021.102306.

[28] Kuroki T, Sakoda N, Shinzato K, Monde M, Takata Y. Dynamic simulation for optimal hydrogen refueling method to Fuel Cell Vehicle tanks. Int J Hydrogen Energy 2018;43:5714–21. https://doi.org/10.1016/j.ijhydene.2018.01.111.

[29] Johnson T, Bozinoski R, Ye J, Sartor G, Zheng J, Yang J. Thermal model development and validation for rapid filling of high pressure hydrogen tanks. Int J Hydrogen Energy 2015;40:9803–14. https://doi.org/10.1016/j.ijhydene.2015.05.157.

[30] Deng S, Li F, Luo H, Yang T, Ye F, Chahine R, Xiao J. Lumped parameter modeling of SAE J2601 hydrogen fueling tests. Sustainability 2023;15:1448. https://doi.org/10.3390/su15021448.

[31] Schneider J, Meadows G, Mathison SR, Veenstra MJ, Shim J, Immel R, Wistoft-Ibsen M, Quong S, Greisel M, McGuire T, et al. Validation and sensitivity studies for SAE J2601. the Light Duty Vehicle Hydrogen Fueling Standard 2014;3. https://doi.org/10.4271/2014-01-1990.

[32] Carrere P, Lodiar G, Vyazmina E, Ammouri F, Charolais A. CFD simulations of the refueling of long horizontal H2 tanks. Int Conf Hydrog Saf 2021:1175–84. Edinburgh.

[33] Kuroki T, Nagasawa K, Peters M, Leighton D, Kurtz J, Sakoda N, Monde M, Takata Y. Thermodynamic modeling of hydrogen fueling process from high-pressure storage tank to vehicle tank. Int J Hydrogen Energy 2021;46:22004. https://doi.org/10.1016/j.ijhydene.2021.04.037. –17.

[34] Melideo D, Baraldi D. CFD analysis of fast filling strategies for hydrogen tanks and their effects on key-parameters. Int J Hydrogen Energy 2015;40:735–45. https://doi.org/10.1016/j.ijhydene.2014.10.138.

[35] Melideo D, Baraldi D, Acosta-Iborra B, Cebolla RO, Moretto P. Cfd investigation of filling and emptying of hydrogen tanks. Proc. Int. Conf. Hydrog. Safety, Yokohama, Japan. 19–21 Oct. 2015. n.d.

[36] Melideo D, Baraldi D, Galassi MC, Ortiz Cebolla R, Acosta Iborra B, Moretto P. Assessment of a CFD model for the simulation of fast filling of hydrogen tanks with pre-cooling. Int Conf Hydrog Saf 2021:1–11.

[37] Heitsch M, Baraldi D, Moretto P. Numerical investigations on the fast filling of hydrogen tanks. Int J Hydrogen Energy 2011;36:2606–12. https://doi.org/10.1016/j.ijhydene.2010.04.134.

[38] Ramasamy V, Richardson ES. Thermal response of high-aspect-ratio hydrogen cylinders undergoing fast-filling. Int J Heat Mass Tran 2020;160:120179. https://doi.org/10.1016/j.ijheatmasstransfer.2020.120179.

[39] Bourgeois T, Ammouri F, Baraldi D, Moretto P. The temperature evolution in compressed gas filling processes: a review. Int J Hydrogen Energy 2018;43:2268–92. https://doi.org/10.1016/j.ijhydene.2017.11.068.

[40] Molkov V, Ebne-Abbasi H, Makarov D. CFD model of refuelling through the entire HRS equipment: the start-up phase simulations. Hydrogen 2023;4:585–98. https://doi.org/10.3390/hydrogen4030038.

[41] Ansys Inc. Ansys Fluent theory guide. 2020.

[42] Launder BE, Spalding DB. The numerical computation of turbulent flows. Comput Methods Appl Mech Eng 1974;3:269–89. https://doi.org/10.1016/0045-7825(74)90029-2.

[43] Lemmon EW, Bell IH, Huber ML, McLinden MO. NIST standard reference Database 23: reference fluid thermodynamic and transport properties-REFPROP, version 10.0. Gaithersburg: National Institute of Standards and Technology, Standard Reference Data Program; 2018. https://doi.org/10.18434/T4/1502528.

[44] Tolias IC, Giannissi SG, Venetsanos AG, Keenan J, Shentsov V, Makarov D, Coldrick S, Kotchourko A, Ren K, Jedicke O, et al. Best practice guidelines in numerical simulations and CFD benchmarking for hydrogen safety applications. Int J Hydrogen Energy 2019;44:9050–62. https://doi.org/10.1016/j.ijhydene.2018.06.005.

[45] Ansys Inc. Ansys® fluent 2020 R2 user manual. 2020. https://ansyshelp.ansys.com/account/secured?returnurl=/Views/Secured/corp/v202/en/. [Accessed 4 February 2023].

[46] Kuroki T, Sakoda N, Shinzato K, Monde M, Takata Y. Prediction of transient temperature of hydrogen flowing from pre-cooler of refueling station to inlet of vehicle tank. Int J Hydrogen Energy 2018;43:1846–54. https://doi.org/10.1016/j.ijhydene.2017.11.033.

[47] Gebhart TMJ, Spiller M, Çelik H, Dahlmann R, Hopmann C. Experimental analyses of the spatial varying temperature development of type-IV hydrogen pressure vessels in cyclic tests considering different length to diameter ratios. Int J Hydrogen Energy 2023;48:27304–18. https://doi.org/10.1016/j.ijhydene.2023.03.353.